JOURNAL OF PROPULSION AND POWER
Vol. 25, No. 2, March–April 2009

Influence of Electrode Shape on Performance of Pulsed Magnetoplasmadynamic Thruster SIMP-LEX

Tony Schönherr,* Anuscheh Nawaz,† Georg Herdrich,‡ Hans-Peter Röser,§ and Monika Auweter-Kurtz¶
Universität Stuttgart, 70569 Stuttgart, Germany

DOI: 10.2514/1.35568

The pulsed magnetoplasmadynamic thruster SIMP-LEX (Stuttgart impulsing magnetoplasmadynamic thruster for lunar exploration) is developed to serve as a main propulsion system for the lunar mission BW1. Optimizing the thruster's performance is necessary to increase the efficiency and the mean exhaust velocity without increasing the system's mass and energy requirements. Results of experiments varying the flare angle and the gap between the electrodes, the applied voltage, as well as using tongue-shaped or rectangular electrodes are shown and evaluated by means of a statistical approach using Taguchi matrices. Furthermore, an analytical approach toward the influence on the change in inductance along the x axis for these parameters was taken and the resulting performance characteristics are presented. Both tongue shape and flare angle, show a positive effect on the performance, that is, impulse bit, mean exhaust velocity, and thrust efficiency. A maximal I_{bit} is given for a flare angle of ≈ 20 deg.

Nomenclature

B	=	magnetic field
C	=	capacitance
c_e	=	mean exhaust velocity
d	=	width of the electrodes
d_e	=	end width of the electrodes
d_0	=	base width of the electrodes
E	=	bank energy
h	=	electrode gap
h_0	=	gap at exit plane of propellant
I	=	current
I_{bit}	=	impulse bit
j	=	current density
L_0	=	initial inductance
l_e	=	free length of electrodes
m_{bit}	=	mass bit
r	=	distance between current filament and integration point
U	=	voltage
x	=	coordinate along the length
x_p	=	plasma position
y	=	coordinate along the width
y'	=	position of the current filament
z	=	coordinate along the gap
α	=	flare angle
γ	=	geometric inclination of magnetic field vector
ΔL	=	change in inductance
η_e	=	electrical efficiency
η_T	=	thrust efficiency
ϑ	=	angle of magnetic field analysis
μ	=	magnetic permeability
μ_r	=	relative magnetic permeability
Φ	=	magnetic flux

Received 12 November 2007; revision received 18 July 2008; accepted for publication 22 October 2008.

*Research Student, Institute of Space Systems, Space Transportation; schoenherr@irs.uni-stuttgart.de.

†Ph.D. Candidate, Institute of Space Systems, Space Transportation; nawaz.anuscheh@googlemail.com.

‡Section Head, Institute of Space Systems, Space Transportation; herdrich@irs.uni-stuttgart.de; Member AIAA.

§Director, Institute of Space Systems; roeser@irs.uni-stuttgart.de.

¶Institute of Space Systems; currently President, Universität Hamburg; praesidentin@hvn.uni-hamburg.de. Fellow Member AIAA.

I. Introduction

THE BW1 mission is the endeavor to send an all electric satellite to the moon. It is part of the Stuttgart Small Satellite Program initiated in 2002 with the aim of lunar exploration [1]. The capacity of power supply and of propellant storage is limited due to the size of the satellite of only 1 m^3 and its mass of approximately 200 kg. The pulsed MPD thruster (iMPD, also known as the pulsed plasma thruster, PPT) SIMP-LEX (Stuttgart impulsing magnetoplasmadynamic thruster for lunar exploration) is developed and investigated as the main propulsion system on this mission due to its low mass and flexible power consumption compared to other electric or chemical alternatives. Additionally, the PPT posed a good option due to the existing heritage from electric thruster design and operation.

An optimal performance of the thruster increases the payload capacity of the satellite. Several geometry variations were investigated for this purpose. Based on other findings, these variations include the geometry of the electrodes, that is, the length, width, and their gap as well as the capacitor voltage [2].

During this study the electrodes were changed in shape, that is, flared and tongue-shaped electrodes were used to increase performance. Referring to research done at other facilities [3–7], the investigation of flared and tongue-shaped electrodes was identified as a good way to raise thrust efficiency, impulse bit, and mean exhaust velocity of the thruster without increasing the mass of the propulsion system, and of the whole satellite, respectively.

Investigations of Meckel et al. [4], Arrington et al. [5], and Kawahara et al. [7] show that an increase in flare angle results in an increase of impulse bit, mean exhaust velocity, and thrust efficiency. Palumbo and Guman [3] found a nonlinearity for these target parameters depending on the flare angle. Therefore, investigating the performance behavior of SIMP-LEX with a changing flare angle is considered to be important for overall thruster optimization.

Antropov et al. [6] found that the thrust efficiency increases by up to 10% for tongue-shaped electrodes compared to rectangular ones.

This paper provides the results obtained from the experimental investigation of SIMP-LEX considering variations in flare angle, electrode shape, applied voltage, and the gap between the electrodes.

II. Thruster and Experimental Setup

SIMP-LEX is a pulsed MPD thruster of about $40 \times 25 \times 10$ cm^3 consisting of four capacitors with a total capacitance of 35 μF. They

are connected in parallel to a pair of copper electrodes. The cathode is equipped with a semiconductor spark plug which serves as the igniter. Figure 1 shows SIMP-LEX and its main parts in its conventional parallel and rectangular setup, whereas Fig. 2 shows a flared and tongue-shaped configuration during operation. The engineering model of SIMP-LEX is built up in such a way that parametric investigations are possible by means of replaceable electrodes and adjustable gap. For the investigations herein, the electrode width and free length were kept constant at 40 mm and 87 mm, respectively. A polytetrafluoroethylene (PTFE) bar is placed between the electrodes as a solid propellant. The capacitor voltage varies between 1500 and 2000 V so that the total energy of the capacitor bank has a range of 40–70 J.

Figure 3 shows a schema of the thruster in a breech-fed configuration with the ablated plasma sheet and the definition of the axes used. Once the capacitors are charged the spark plug triggers and forms a short-time arc discharge. This discharge ionizes the propellant along the surface causing a discharge of the main circuit. The ablated and ionized propellant forms a conductive plasma sheet. This circuit forms a current loop that creates a magnetic field. The magnetic field perpendicular to the plasma current leads to a Lorentz force accelerating the plasma. Hence, an impulse is achieved by the thruster. One pulse ends when the entire energy stored in the capacitor is discharged. The duration of the discharge depends on the electrical properties of the oscillation circuit and is about 30 μs as

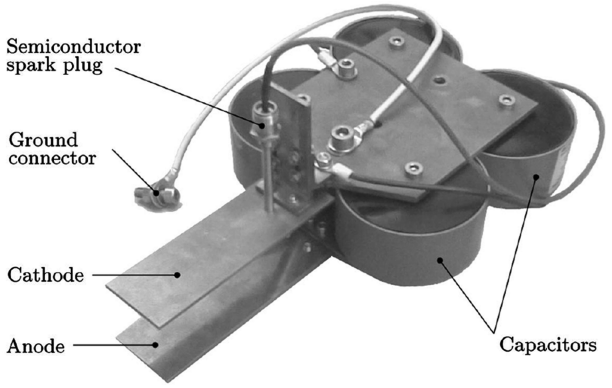

Fig. 1 Setup of SIMP-LEX.

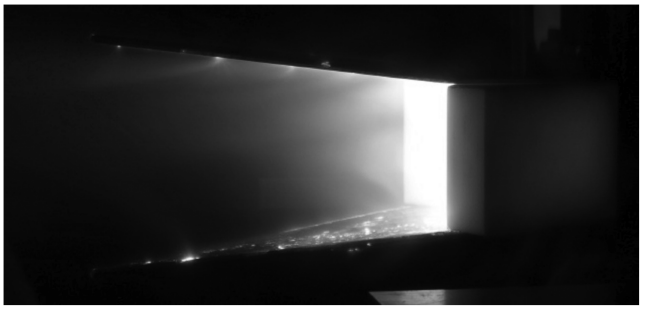

Fig. 2 SIMP-LEX during one pulse for flared, tongue-shaped electrode configuration.

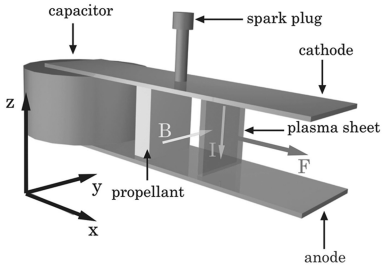

Fig. 3 Working principle of SIMP-LEX.

can be derived from the voltage measured between the capacitors. An example of a voltage progression is shown in Fig. 4.

The vacuum chamber used for the experimental investigation provides a pressure environment of 4×10^{-4} mbar and is equipped with a balance to measure the impulse bit created by the thruster [2] as shown in Fig. 5. The thruster's semiconductor igniter is triggered through an electronic box mounted on a pendulum structure. The capacitor voltage is adjustable and is fed through the torsion spring suspension. This means that no cable is connected with the moving part of the pendulum leading to an almost frictionless setup (damping constant <0.01 1/s).

At the bottom of the pendulum frame, a scale is attached and opposing this scale, an optical sensor is installed. By emitting an infrared signal on the scale and by measuring the reflection, the sensor records contactlessly the deflection of the pendulum with a resolution of 50 nm corresponding to about 0.1% of the measured signal. Based on a calibration using the theory of ideal energy conversion the impulse bit is derived from the average of the deflection of 10 measurements leading to a conservative value of the impulse. The maximum error for the impulse bit is 11%. An eddy current brake is installed to restrict the oscillation of the pendulum before and after each impulse measurement. The brake is switched off when measuring the deflection.

The ablated mass bit per pulse for each experiment is determined by measuring the weight of the propellant bars before and after a known number of pulses using a balance with a resolution of 100 μg for a mass less than 240 g. For the experiments conducted between 200 and 650 pulses were ignited to minimize uncertainties yielding a standard error of 6%.

From the impulse bit I_{bit} and the mass bit m_{bit}, the mean exhaust velocity c_e and the thrust efficiency η_T can be calculated easily:

$$c_e = \frac{I_{\text{bit}}}{m_{\text{bit}}} \tag{1}$$

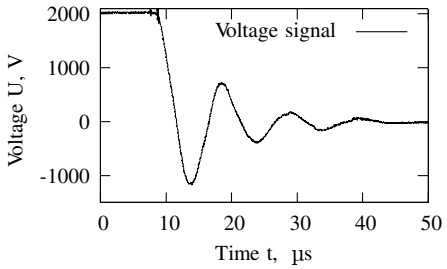

Fig. 4 Voltage signal recorded for SIMP-LEX.

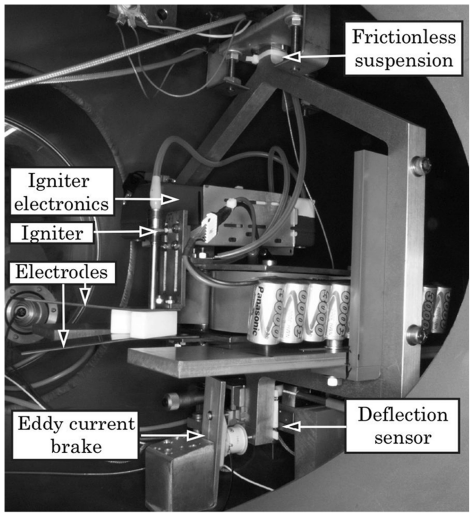

Fig. 5 Impulse bit measurement using a thrust balance.

Table 1 Investigated parameters and their levels

	Parameter	Levels
A	Flare angle α, deg	0, 10, 20, 30
B	Electrode shape	Rectangular (R), tongue (T)
C	Electrode gap h, mm	21, 36
D	Voltage U, V	1500 (1.5 kV), 2000 (2 kV)

$$\eta_T = \frac{I_{\text{bit}}^2}{2 \cdot m_{\text{bit}} \cdot E_0} \tag{2}$$

where E_0 equals the stored bank energy of the capacitors $\frac{1}{2}CU^2$ with the capacitance C and the voltage U. Resulting from the law of error propagation, the mean exhaust velocity and the thrust efficiency are affected by standard errors of 12 and 22%, respectively.

III. Test Matrix

For determination and analysis of the experiments, a statistical approach named the Taguchi method [8] was taken. The basic idea of this method is the use of statistics for the evaluation of influences of parameters and their interactions on a characteristic value. The full range of permutations is not necessary for this investigation. Hence, the introduction of the method allows for determination of the influences while efficiently reducing the number of experiments necessary. However, the method is limited due to nonlinear progressions between parameter levels and confounding of parametric effects. The choice of the parameters and the definition of their levels requires good engineering judgment to allow interpretation of the results. For the four parameters investigated, a so-called Taguchi matrix was created calling for several permutations of the experimental setup. This type of approach has already been used on other iMPD thrusters [4]. Table 1 shows the parameters considered and their levels that have been taken into account in this study.

Considering the number of possible permutations, $n_{\text{total}} = 4 \times 2 \times 2 \times 2 = 32$ experiments would be necessary by investigating conventionally. When associating the parameters from Table 1 to the columns of the Taguchi matrix, the four-level parameter of the flare angle is listed in three columns. Further, the Taguchi matrix yields interactions between parameters, for example, the interaction between gap (C) and voltage (D) is associated with a separate column CD. Figure 6 shows the empty test matrix to which the parameters have been linked.

The first column states the trial number. The second column of the matrix is used for the value obtained from the different trial setups, that is, I_{bit}, m_{bit}, c_e, and η_T. This value is then copied along the row. A gray field means no entry. Each parameter is split up in two subcolumns referring to the two levels. For example, column B is split up into rectangular (R) and tongue-shaped (T) electrode configurations. The mean value of each subcolumn is then calculated, and the difference between two pertinent subcolumns relates to the effect in the last row when changing the parameter from a low to a high level. This effect contains an error as a result of the errors of the 16 values measured due to the error propagation yielding a careful interpretation of the values obtained.

Because the flare angle was investigated for not only two but four levels, it has to be treated as shown in Fig. 7. The different levels of flare angle are reached by combining columns 1 and 2, for example, a high level in column 1 and a low level in column 2 results in a flare angle of 20 deg. Column 5 represents the interference of columns 1 and 2, that is, also the main effect of the flare angle even though it is not related to a physical flare angle. This means that interpretation of the results has to consider all three columns in order to draw a conclusion on the influence of the flare angle.

From the Taguchi matrix in Fig. 6 the 16 experiments necessary are derived as summarized in Table 2.

To allow a closer investigation of the nonlinear effect of the flare angle on the target values, additional experiments were considered to be undertaken as found in Table 3.

The Taguchi matrix was used to determine the influence of the parameters on the measured values, impulse bit and mass bit, and the calculated values, mean exhaust velocity, and thrust efficiency, respectively.

IV. Theoretical Investigation

The accelerating component of the magnetic field B_y between the electrodes of the thruster can be calculated for a single current filament using Ampère's law for current filaments of infinite length considering Fig. 8:

$$B_y = \frac{\mu j}{2\pi r} \cos\gamma \tag{3}$$

where the angle between the magnetic field vector **B** and the y axis along the width of the electrodes is defined by $\cos\gamma = \frac{z}{r}$ and the

	1 A	2 A	5 A
0°			
10°			
20°			
30°			

Fig. 7 Flare angle levels.

Trial number	Value	1 A	2 A	3 B	4 C	5 A	6 AB	7 AC	8 AB	9 AC	10 BC	11 CD	12 BD	13 AD	14 AD	15 D
				R T	21 36											1.5 2
1																
2																
3																
4																
5																
6																
7																
8																
9																
10																
11																
12																
13																
14																
15																
16																
Total	0	0 0	0 0	0 0	0 0	0 0	0 0	0 0	0 0	0 0	0 0	0 0	0 0	0 0	0 0	0 0
Values	16	8 8	8 8	8 8	8 8	8 8	8 8	8 8	8 8	8 8	8 8	8 8	8 8	8 8	8 8	8 8
Mean	0	0 0	0 0	0 0	0 0	0 0	0 0	0 0	0 0	0 0	0 0	0 0	0 0	0 0	0 0	0 0
Effect		0	0	0	0	0	0	0	0	0	0	0	0	0	0	0

Fig. 6 Empty Taguchi matrix.

Table 2 Parameter matrix for the experimental investigation

Trial no.	Flare angle, deg	Shape	Gap, mm	Voltage, V
1	0	Rectangular	21	2000
2	0	Rectangular	36	1500
3	0	Tongue	21	1500
4	0	Tongue	36	2000
5	10	Rectangular	21	1500
6	10	Rectangular	36	2000
7	10	Tongue	21	2000
8	10	Tongue	36	1500
9	20	Rectangular	21	1500
10	20	Rectangular	36	2000
11	20	Tongue	21	2000
12	20	Tongue	36	1500
13	30	Rectangular	21	2000
14	30	Rectangular	36	1500
15	30	Tongue	21	1500
16	30	Tongue	36	2000

Table 3 Additional tests for investigation of nonlinearity

Trial no.	Flare angle, deg	Shape	Gap, mm	Voltage, V
4a	0	Rectangular	36	2000
6b	10	Tongue	36	2000
10b	20	Tongue	36	2000
16a	30	Rectangular	36	2000

distance between the current filament and the point of investigation is $r = \sqrt{(y - y')^2 + z^2}$. The variables y and z are the coordinates of the point of investigation, y' defines the position of the current filament, and μ equals the magnetic permeability (with relative permeability $\mu_r = 1$). The current density j results from the distribution of the total current I across the width d.

The total component of the magnetic field $B_{y,\text{tot}}$ can then be calculated by integrating across the width:

$$B_{y,\text{tot}}(y,z) = -\frac{\mu I}{2\pi d}\int_0^d \frac{z}{(y-y')^2+z^2}\,\mathrm{d}y' = -\frac{\mu I}{2\pi d}\left[\arctan\left(\frac{y}{z}\right) + \arctan\left(\frac{d-y}{z}\right)\right] \tag{4}$$

Integration of the magnetic field over the area $\mathrm{d}x\,\mathrm{d}z$ results in the magnetic flux Φ for the position x_p:

$$\Phi(x_p, y) = \int_0^h \int_0^{x_p} \frac{\mu I}{2\pi d}(\vartheta_1 + \vartheta_2)\,\mathrm{d}x\,\mathrm{d}z \tag{5}$$

Here, ϑ_1 is equal to the solution of the integral of Eq. (4) and ϑ_2 equals the solution of this integral for the opposite electrode:

$$\vartheta_1 = \arctan\left(\frac{y}{z}\right) + \arctan\left(\frac{d-y}{z}\right) \tag{6}$$

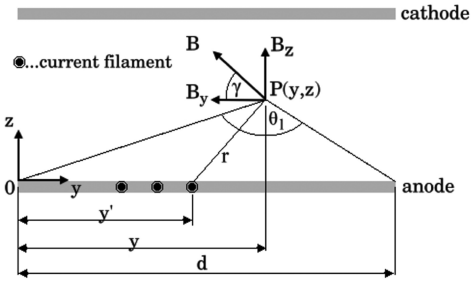

Fig. 8 Calculation of the magnetic field for one current filament (upstream view).

$$\vartheta_2 = \arctan\left(\frac{y}{h-z}\right) + \arctan\left(\frac{d-y}{h-z}\right) \tag{7}$$

To obtain processable values, the magnetic flux is averaged along the width of the electrodes:

$$\bar{\Phi}(x_p) = \frac{1}{d}\int_0^d \int_0^h \int_0^{x_p} \frac{\mu I}{2\pi d}(\vartheta_1 + \vartheta_2)\,\mathrm{d}x\,\mathrm{d}z\,\mathrm{d}y \tag{8}$$

In the case of flared and tongue-shaped electrodes, the parameters d and h are no longer constant, but a function of the axial coordinate x. Therefore, it is necessary to rearrange the integration steps to consider influence of the electrode shape in the magnetic flux and to permit a full integration, that is, integrating first over z, then y and finally x.

The functions describing the gap between the electrodes $h(x)$ and the electrode width $d(x)$ are found regarding Figs. 9 and 10 respectively:

$$h(x) = h_0 + 2 \cdot \tan\left(\frac{\alpha}{2}\right) \cdot x \tag{9}$$

$$d(x) = d_0 \cdot \left(1 - \frac{x}{l_e}\right) + d_e \cdot \frac{x}{l_e} \tag{10}$$

In these functions, h_0 refers to the height of the propellant bars, and the angle between the x axis and the electrodes is the flare angle α. For the width, d_0 equals the width at the base of the electrodes, l_e the free length of the electrodes measured from the propellant surface, and d_e the width of the electrodes at their end.

Integration of Eq. (8) over y and z could be solved analytically using a mathematical solver. The integration over x was solved numerically:

$$\bar{\Phi}(x_p) = \frac{\mu I}{2\pi} \cdot \int_0^{x_p} f[x, d(x), h(x)]\,\mathrm{d}x \tag{11}$$

The mean change in inductance $\Delta\bar{L}$ of the electric circuit as the function of the position of the plasma sheet x_p can be calculated by dividing the mean magnetic flux by the current, yielding

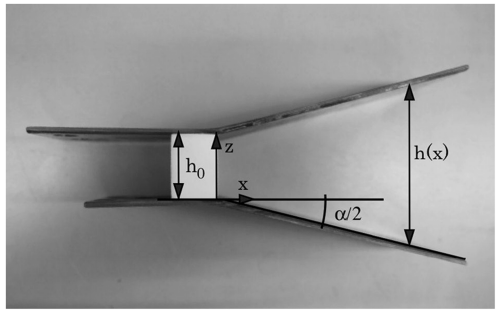

Fig. 9 Geometry of flared electrodes.

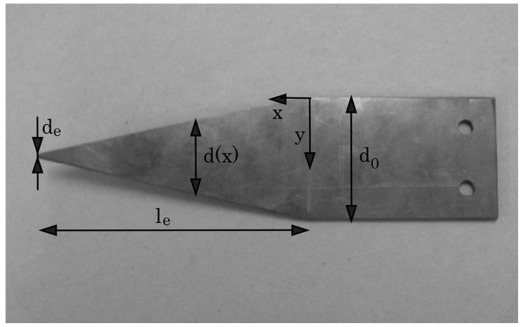

Fig. 10 Geometry of tongue-shaped electrodes.

$$\Delta\bar{L}(x_p) = \frac{\bar{\Phi}(x_p)}{I} = \frac{\mu}{2\pi} \cdot \int_0^{x_p} f[x, d(x), h(x)]\,\mathrm{d}x \qquad (12)$$

Numerical investigations were performed to assess the influence of the flare angle and electrode shape on this change in inductance. For this, $\Delta\bar{L}$ was calculated along the electrode length for each plasma position varying the electrode shape or the flare angle and plotting over this position. Concerning the tongue-shaped electrodes the width at the end of the electrodes d_e was varied. A width of 100% of d_0 refers to rectangular electrodes, and 0% of d_0 to fully tongue-shaped electrodes, as seen in Fig. 10. The results of these calculations are presented in Figs. 11 and 12.

The change in inductance with the position of the plasma increases with higher flare angles as well as with a lower end width. For positions close to the propellant bar the difference due to flare angle and tongue shape is negligible. At the end of the electrodes the differences are very high. In case of pointed electrodes (0% d_0) the change in inductance tends toward infinity which is due to the singularity of the magnetic field in the electrode tip.

This increase improves the electrical performance of the thruster circuit which can be derived regarding the inequality of the electrical efficiency η_e [9]:

$$\eta_e < \frac{\Delta L}{L_0} \qquad (13)$$

where L_0 refers to the initial inductance.

Keeping L_0 at the same value defined by the geometry of the thruster, the upper boundary of the electric efficiency rises with an increase in ΔL which also motivates an experimental proof of this theoretical conclusion.

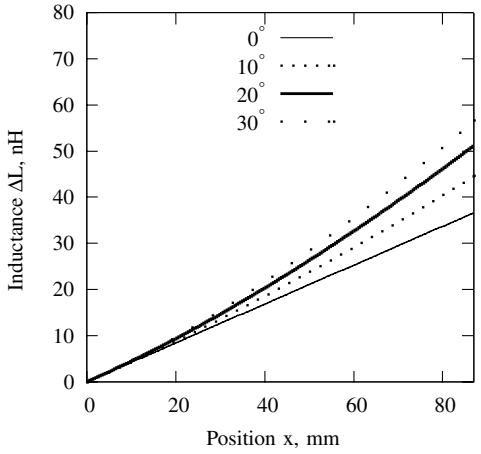

Fig. 11 Change in inductance for different flare angles and rectangular electrodes.

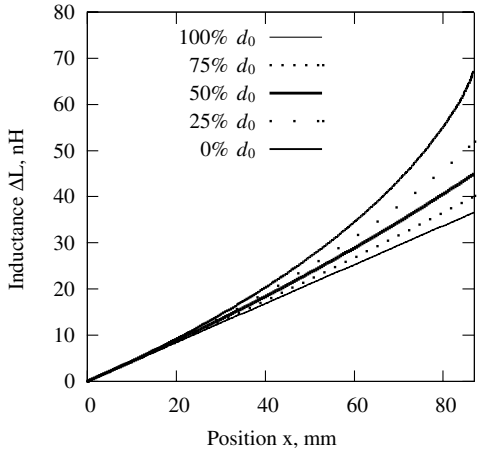

Fig. 12 Change in inductance for different end widths and parallel electrodes.

V. Experimental Results

For each experiment conducted, the impulse bit and the mass bit was derived from the values measured, and the mean exhaust velocity and the thrust efficiency calculated. Although the results are processed with the Taguchi method, some benchmark configurations and their performance characteristics are listed in Table 4 to provide information about the obvious improvement.

A. Results of Taguchi Matrices

Processing the results of the experiments listed in Table 2 leads to the following results in the Taguchi matrix. Table 5 represents the last line "effect" of the related matrix in Fig. 6. A positive value indicates a positive effect on the investigated parameter while changing the parameter level from "low" to "high." The higher the number the bigger this effect. Columns 1–5 and 15 show the main effects of the parameters and the other columns present the two-parameter interaction effects, for example, column 12 = BD shows the effect of the coupling of parameters B = shape and D = voltage.

It can be seen that the main parameters accountable for an increase in the impulse bit are capacitor voltage (column 15) and electrode gap (column 4). Furthermore, the interaction between gap and voltage plays a significant role (column 11 = CD). This means that an increase of both values at the same time causes an additional increase in impulse bit. An increased gap causes higher mass bits due to a larger propellant surface and an increase in voltage causes a higher exhaust velocity; hence the impulse bit is strongly affected by changes of both parameters.

All three columns linked to the flare angle (columns 1, 2, and 5 = A) show that the impulse bit decreases when increasing the angle. To further investigate this effect, the Taguchi matrix in Fig. 6 can be split up into smaller matrices, each linked to a step in the flare angle of 10 deg. These matrices are based on the same statistical theory yielding a better understanding of the phenomena linked to a change in flare angle. For all three steps, the effects of the pertinent column of the flare angle are presented in Table 6.

From these results, it is obvious that, on average, the flare angle only has a positive effect on the thruster's performance, that is, the impulse bit, the mean exhaust velocity, and the thrust efficiency, when raised from 0 to 20 deg. Changing the flare angle from 20 to 30 deg decreases the performance.

Changing the shape of the electrodes in column 3 (B) of Table 5 also increases the impulse bit. Even though the increase is smaller than for the gap between the electrodes and the applied voltage, it can be seen as proof that the thruster performance is ameliorated through an increase of change in inductance due to shape changes.

Most other interactions seem to be negligible. Column 10 of the impulse bit shows a negative interaction between the shape and the gap. This could be caused by improper acceleration of the plasma along the electrodes, as the gap-to-width ratio increases along the acceleration path.

For the mass bit, the same conclusions can be drawn. Voltage and gap increase the amount of ablated mass. However, this time neither the electrode shape nor the interaction of gap and voltage seem to have an effect on the mass bit.

A higher impulse bit increases the mean exhaust velocity whereas a higher mass bit reduces it. These trends are combined in the results of the Taguchi matrix for the mean exhaust velocity. Confirming previous studies [4], it can be seen that a larger gap (C) has a negative effect on the mean exhaust velocity. Even though the impulse bit is raised, the larger ablation surface causes the ablated plasma to be accelerated less. Raising the voltage (D) causes an increase in mean exhaust velocity. The interaction of voltage and gap (CD) shows the highest raise in mean exhaust velocity of all parameters which is due to the positive interaction effect on the impulse bit as discussed previously.

Table 4 Experimental results for a fraction of the test matrix

Trial	U, V	h, mm	α, deg	Shape	I_{bit}, μNs	m_{bit}, μg	c_e, km/s	η_T, %
1	2000	21	0	Rectangular	1340	137	9.8	9.7
7	2000	21	10	Tongue	1380	120	11.4	10.8
10b	2000	36	20	Tongue	1960	168	11.7	16.7

Table 5 Results of measurements (I_{bit} in μNs, m_{bit} in μg, c_e in km/s, η_T in %)

		1 A	2 A	3 B	4 C	5 A	6 AB	7 AC	8 AB	9 AC	10 BC	11 CD	12 BD	13 AD	14 AD	15 D
Effect	I_{bit}	−4	−61	52	327	−94	37	32	−2	21	−24	218	22	−39	−21	632
Effect	m_{bit}	−0.7	−3.7	−2.8	44.6	−1.4	3.6	0.4	−0.6	2.6	2.9	−1.9	−5.6	4.1	−0.4	44.5
Effect	c_e	0.0	−0.1	0.6	−1.3	−0.7	0.2	0.2	0.0	−0.1	−0.4	1.9	0.6	−0.6	−0.1	1.1
Effect	η_T	0.5	−0.4	0.9	1.2	−1.3	0.6	0.4	0.1	0.1	−0.4	3.5	0.6	−0.9	−0.3	0.6

Table 6 Effects of the flare angle regarding each step

0–10 deg	1
	A
I_{bit}	33.0
m_{bit}	−2.3
c_e	0.6
η_T	0.9
10–20 deg	1
	A
I_{bit}	57.0
m_{bit}	3.0
c_e	0.1
η_T	0.9
20–30 deg	1
	A
I_{bit}	−155.0
m_{bit}	−5.0
c_e	−0.8
η_T	−1.7

Apparently the improved shape of the electrodes increases the velocity slightly whereas the flare angle seems to have a negative effect on the performance.

The thrust efficiency shows similar tendencies as the impulse bit. Astonishingly, the voltage seems to have no effect on the efficiency. However, for the interaction between gap and voltage (CD) an extremely high positive value was found, that is, the combination of the parametric changes yields an improved intake of electric power of the PTFE plasma. Shape (B) and electrode gap (C) have a positive effect on the efficiency. Most other interaction effects can be neglected. The values for the effects influencing the thrust efficiency have to be considered carefully, as they are affected by both, the errors due to the measurement already propagated to the value of each configuration and the error due to the propagation when calculating the effect out of the 16 values. For the values measured, an error of ± 1.1 percentage points can be calculated affecting each effect.

Within all experiments performed the following configurations showed best performance: configuration 10b (20 deg tongue, 36 mm, 2000 V) had the highest impulse bit $I_{\text{bit}} = 1960\ \mu\text{N}\cdot\text{s}$ and the best thrust efficiency $\eta_T = 16.7\%$ while configuration 6b (10 deg tongue, 36 mm, 2000 V) had the highest mean exhaust velocity $c_e = 11.9$ km/s.

B. Nonlinearity Investigation

The approach using Taguchi matrices works well for linear dependancies. To investigate nonlinearities within the range of the parameters additional experiments were performed. These tests, summarized in Table 3, are not part of the Taguchi matrix and were not discussed within the previous section.

All experiments for this investigation were undertaken at one voltage, 2000 V, and one gap, 36 mm. Only variations of shape and especially flare angle were considered. Figures 13–16 show the results of these measurements along with their error bars (simple standard error).

As seen in Fig. 13, the impulse bit decreases above a flare angle of 20 deg. For 30 deg it even reaches a lower level than for the parallel configuration at 0 deg. In this case the divergent form probably causes the plasma to separate from the electrodes and the acceleration is reduced. For the same reason the mean exhaust velocity and the thrust efficiency are reduced for higher flare angle irrespective of the shape of the electrodes.

This sudden decrease after the curve's maximum at $\approx$20 deg causes the confusing values of the Taguchi matrix in columns 1, 2, and 5 regarding the flare angle influence as the matrix expects linear functions. The flare angle has a positive effect on the overall thruster performance for a flare angle up to about 20 deg and may be regarded for optimizing an iMPD.

Even though the simple standard error of the results is higher than the variation of the performance with flare angle and electrode shape, the preceding section showed the positive influences of this change in electrode design when averaged over all configurations. The charts

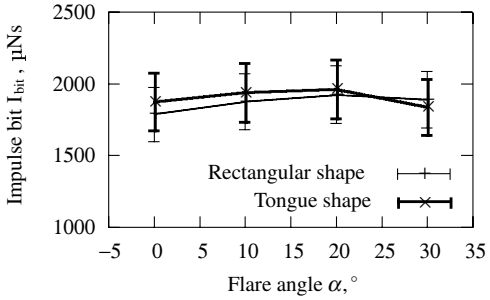

Fig. 13 Impulse bit over flare angle.

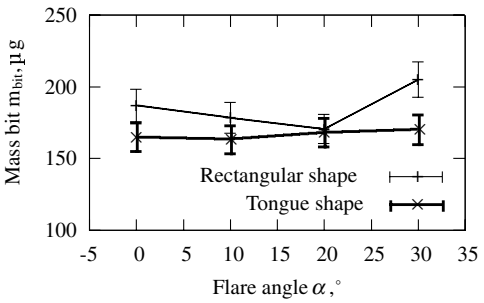

Fig. 14 Mass bit over flare angle.

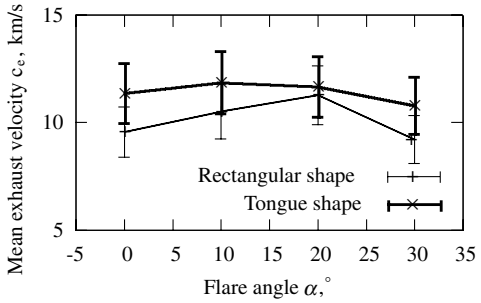

Fig. 15 Mean exhaust velocity over flare angle.

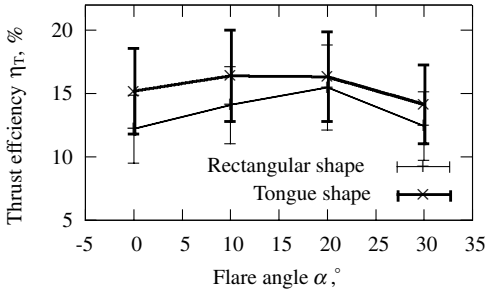

Fig. 16 Thrust efficiency over flare angle.

shown represent the values obtained for only one configuration of voltage and gap.

VI. Conclusions

Comparison of the results obtained through the experimental work with research at other facilities shows a very good correspondence. An increase in impulse bit and exhaust velocity with higher flare angle was indicated in former experiments [3–5,7] and is also used for other flight models [10]. This increase in performance could be verified for the pulsed MPD thruster SIMP-LEX. The sudden decrease of performance for a flare angle higher than 20 deg had also been observed by Palumbo and Guman [3] even though the energy level of their investigation at 450–700 J was much higher. This means that the effect occurs not only for one configuration and setup. The performance maximum at a flare angle of about 20 deg may then be a general property of the iMPD thruster. Further experiments will be necessary to determine the exact maximum. However, in all experiments conducted the tongue shape showed a positive effect on the investigated characteristics.

Increasing the flare angle to 20 deg and shaping the electrodes to a tongue showed an increase of the thrust efficiency by nearly 35% (comparing configurations 1 and 11), much higher than the assumed 5–10% observed by Antropov et al. [6].

Furthermore, general tendencies concerning the increase in impulse bit, the mean exhaust velocity, and the thrust efficiency observed by Meckel et al. [4] and Arrington et al. [5] could be confirmed. The change in performance due to electrode shape and flare angle lies within the error resulting from the experimental setup. Even so, on average, an increase in performance could be observed with the 20 deg flared and tongue-shaped configuration. As SIMP-LEX is foreseen as a long-term propulsion system, it benefits from the average raise in performance parameters.

The influence of the electrode shape was also analyzed by calculating the change in inductance resulting from the geometry varied. The results predict an increase in the upper boundary of the electrical efficiency yielding a possible increase in performance. Further, the progressions will be inputted into the numerical model to describe the thruster's behavior analytically [11].

The configuration with highest mean exhaust velocity (11.9 km/s) was found for a high gap $h = 36$ mm and high voltage $U = 2000$ V configuration for a width of the electrodes of 40 mm. Preliminary investigations [2] showed an increase in mean exhaust velocity when reducing the width of the electrodes. It is therefore interesting for future experiments to decrease the width d further while increasing the gap h and voltage U to see if an additional increase in the mean exhaust velocity can be obtained for configurations with tongue-shaped and flared electrodes. Subsequent work should also consider the verification of the observable strong interaction effect between h and U (CD) on the mean exhaust velocity and the thrust efficiency.

Acknowledgments

This work is funded by the Deutsches Zentrum für Luft- und Raumfahrt (DLR) under contract number FKZ-50-JR-0446. The support regarding discussions of experimental results with Matthias Lau and the experimental help from Bastian Steiner is well acknowledged. T. Schönherr wants to express his most sincere gratitude to Anuscheh Nawaz for the possibility to publish and the outstanding supervision.

References

[1] Laufer, R., Röser, H.-P., and the Lunar Mission BW1 Project Team, "The Stuttgart Moon Orbiter Lunar Mission BW1," *First CEAS European Air and Space Conference Century Perspectives* [CD-ROM] Sept. 2007.

[2] Nawaz, A., Herdrich, G., Kurtz, H., Schönherr, T., and Auweter-Kurtz, M., "SIMP-LEX: Systematic Geometry Variation Using Thrust Balance Measurements," International Electric Propulsion Conference Paper 07-168, Sept. 2007.

[3] Palumbo, D. J., and Guman, W. J., "Effects of Propellant and Electrode Geometry on Pulsed Ablative Plasma Thruster Performance," *Journal of Spacecraft and Rockets*, Vol. 13, No. 3, March 1976, pp. 163–167. doi:10.2514/3.57077

[4] Meckel, N. J., Hoskins, W. A., Cassady, R. J., Myers, R. M., Oleson, S. R., and McGuire, M. L., "Improved Pulsed Plasma Thruster Systems for Satellite Propulsion," AIAA Paper 96-2735, July 1996.

[5] Arrington, L. A., Haag, T. W., Pencil, E. J., and Meckel, N. J., "A Performance Comparison of Pulsed Plasma Thruster Electrode Configurations," International Electric Propulsion Conference Paper 97-127, Aug. 1997; also NASA TM 97-206305.

[6] Antropov, N. N., Diakonov, G., Orlov, M., Popov, G. A., Tyutin, V., and Yakovlev, V., "Development and Refinement of Highly Efficient 150 J APPT," International Electric Propulsion Conference Paper 03-061, March 2003.

[7] Kawahara, K., Kumagai, N., Sato, K., Tamura, K., Koide, T., Harima, K., Fukushima, T., and Takegahara, H., "Study on Plume Characteristics of Pulsed Plasma Thruster," International Electric Propulsion Conference Paper 03-160, March 2003.

[8] Lochner, R. H., and Matar, J. E., *Designing for Quality: An Introduction to the Best of Taguchi and Western Methods of Statistical Experimental Design*, Quality Resources, White Plains, NY, 1st ed., 1990.

[9] Jahn, R. G., *Physics of Electric Propulsion*, Dover, Mineola, NY, 2006, p. 265.

[10] Popov, G. A., and Antropov, N. N., "Ablative PPT. New Quality, New Perspectives," *Acta Astronautica*, Vol. 59, Nos. 1–5, July–Sept. 2006, pp. 175–180. doi:10.1016/j.actaastro.2006.02.009

[11] Nawaz, A., Bauder, U., Böhrk, H., Herdrich, G., and Auweter-Kurtz, M., "Electrostatic Probe and Camera Measurements for Modeling the iMPD SIMP-LEX," AIAA Paper 2007-5280, July 2007.

E. Choueiri
Associate Editor